Lab on a Chip

PAPER

View Article Online
View Journal

Cite this: DOI: 10.1039/d5lc00834d

Microfluidic compartmentalization reveals that ferrostatin-1 restores directional mitochondrial transport in Aβ-challenged neurons

Nad'a Majerníková, [ab] Beatrice Corci, [cd] Yuequ Zhang, [a] Tingting Chen, [a] Maaike van Koeveringe, [a] Denice Mensinga,[ac] Patty P. M. F. A. Mulder, [c] Elisabeth Verpoorte, [c] Andrea Mattarei, [e] Diana Pendin, [ef] Cristina Mammucari, [f] Christoffer Åberg, [c] Wilfred den Dunnen [b] and Amalia M. Dolga *[ab]

Mitochondrial dysfunction is a hallmark of neurodegenerative diseases, including Alzheimer's disease (AD). While ferroptosis has been implicated in AD through iron accumulation and amyloid β (Aβ)-mediated toxicity, its role in mitochondrial regulation remains unclear. Here, we examined whether mitochondrial dysfunction in AD increases neuronal vulnerability to ferroptosis and whether ferroptosis inhibition can preserve mitochondrial network integrity. Primary cortical neurons were cultured in a multi-compartment microfluidic platform that facilitated high-resolution tracking of mitochondrial dynamics using time-lapse microscopy. Prolonged exposure to the ferroptosis inducer erastin disrupted neuronal networks, whereas acute exposure to erastin or Aβ significantly enhanced retrograde mitochondrial transport. These effects were blocked by the ferroptosis inhibitor ferrostatin-1 (Fer-1). Using a novel mitochondrial calcium probe (mt-Fura 2.3 AM), we further demonstrated that Aβ acutely increased mitochondrial calcium, which was ameliorated by Fer-1 and by inhibition of the mitochondrial calcium uniporter with MCUi4. In contrast, Aβ-induced hyperactivity recorded on a microelectrode array was prevented by MCUi4, but not Fer-1. Together, these results show that ferroptotic stress profoundly impacts mitochondrial movement and calcium regulation in neurons. Our multimodal microfluidic approach establishes a direct mechanistic link between ferroptosis, mitochondrial dysfunction, and neuronal vulnerability in AD, offering new insights into therapeutic targeting of ferroptosis in neurodegeneration.

Received 1st September 2025,
Accepted 7th April 2026

DOI: 10.1039/d5lc00834d

rsc.li/loc

Introduction

Alzheimer's disease (AD) is the most prevalent form of dementia for which an effective treatment is missing.[1] Important pathological hallmarks of AD include amyloid β (Aβ), and tau hyper phosphorylation (p-tau) leading to formation of neurofibrilary tangles (NFTs).[2,3] These extracellular and intracellular aggregates induce neurotoxicity and cell death resulting in brain degeneration and cognitive decline.[4] Apart from Aβ and NFTs, mitochondrial dysfunction is an early event in the pathophysiology of AD.[5] Current evidence supports mitochondrial dysfunction being linked to mild cognitive impairment (MCI), which could precede AD progression.[6,7] AD-related mitochondrial damage has been reported in the form of disrupted mitochondrial structure and biogenesis, altered axonal mitochondrial transport, altered mitochondrial calcium signaling, and decrease of mitochondrial membrane potential.[8–11]

Ferroptosis, iron accumulation-related and lipid peroxidation-driven type of programmed cell death, has been suggested to play a role in neurodegeneration.[12–16] In AD, metals like iron interact with amyloid precursor protein (APP) leading to increased Aβ production.[17–19] Aβ oligomers cluster at synapses, where they can interact with the *N*-methyl-D-aspartase receptor (NMDAR) and the metabotropic glutamate receptor 5 (mGluR5), which can lead to an increase in intracellular calcium (Ca^{2+}).[20,21] Aβ can also bind to the cell membrane directly and act as an ion channel, that can exacerbate the cellular intake of calcium.[22] Additionally, Ryanodine receptors (RyRs) are overactive in AD, resulting in increased calcium release from the ER,

[a] *Department of Molecular Pharmacology, Groningen Research Institute of Pharmacy, University of Groningen, Groningen, The Netherlands. E-mail: a.m.dolga@rug.nl*
[b] *Department of Pathology and Medical Biology, University Medical Center Groningen, Groningen, The Netherlands*
[c] *Department of Pharmaceutical Analysis, Groningen Research Institute of Pharmacy, University of Groningen, Groningen, The Netherlands*
[d] *Polymer Science, Zernike Institute for Advanced Materials, University of Groningen, Groningen, The Netherlands*
[e] *Department of Pharmaceutical and Pharmacological Sciences, University of Padua, 35131 Padua, Italy*
[f] *Department of Biomedical Sciences, University of Padua, 35131 Padua, Italy*

which might contribute to ferroptosis.[18,23,24] The mitochondrial calcium uniporter (MCU) plays a crucial role in buffering increased Ca^{2+} levels, but excessive calcium uptake can lead to Ca^{2+} overload and mitochondrial dysfunction.[25] Mitochondrial health is maintained in part through proper mitochondrial movement, which occurs in both anterograde and retrograde directions.[26] Notably, increased retrograde transport has been linked to the removal of aged or damaged organelles *via* mitophagy,[27] a process that is impaired in AD.[28,29] This impaired mitophagy may contribute to dysfunctional mitochondrial dynamics, which could further exacerbate amyloid-β accumulation and toxicity in AD pathology.[30] Furthermore, Aβ stimulates glutamate release into the synapses, as well as inhibiting the reuptake.[31] This leads to inhibition of the glutathione (GSH) pathway, eventually leading to decreased glutathione peroxidase 4 (GPx4) activity, which plays an important role in ferroptosis being able to reduce Aβ aggregation.[32,33] Finally, significant reduction of GSH levels was observed in the brain of patients with MCI compared to healthy control subjects.[7,34] Altogether these findings indicate that mitochondrial dysfunction could be a common denominator of mechanisms involved in the development of AD-related Aβ toxicity and ferroptosis.

Here, we investigated the effects of ferroptosis modulation on primary cortical neurons (PCNs) challenged by an ferroptosis inducer, tracking mitochondrial movement and calcium signaling, as well as, neuronal activity in the context of Aβ treatment. We employed a two-compartment microfluidic system, that enabled us to selectively treat neuronal compartments and precisely track directional mitochondrial transport, thereby providing a physiologically relevant model to assess how Aβ and ferroptosis inducers affect axonal integrity and neuronal network function. Our results suggest that reducing ferroptosis vulnerability could restore AD-related alterations in mitochondrial movement, and mitochondrial calcium signaling.

Methods

Cell culture

We used mouse hippocampal-derived neuronal-like cell line (HT-22)[35,36] in Dulbecco's modified Eagle medium (DMEM; #42430025; Gibco, Thermo Fisher Scientific, Netherlands) supplemented with 10% fetal bovine serum (FBS; #SV3016.03; Hyclone, USA), 100 U ml^{-1} penicillin, 100 μg ml^{-1} streptomycin (#15070-063; Gibco, Thermo Fisher Scientific, Netherlands), and 1% sodium pyruvate (#11360-070; 100 mM; Gibco, Thermo Fisher Scientific, Netherlands) at 37 °C and 5% CO_2. Cells were mycoplasma free and their passage number ranged between 270 and 350.

Primary cortical neurons (PCN) were prepared from C57BL/6 embryonic (E13-14) mice (mixed sex) under sterile conditions.[37] All animal procedures were performed in accordance with the Guidelines for Care and Use of Laboratory Animals of the University of Groningen, the Netherlands and approved by the Animal Experiments Committee (DEC). The cortices from embryos were collected, treated with 0.2 mg ml^{-1} trypsin and DNase at 37 °C for 15 min, and centrifuged to obtain the cell pellet. The pellet was re-suspended in neurobasal medium (#2508186; Gibco, Thermo Fisher Scientific, Netherlands) supplemented with 100 U ml^{-1} penicillin, 100 μg ml^{-1} streptomycin (#15070-063; Gibco, Thermo Fisher Scientific, Netherlands), 2 mM L-glutamine (#15070063; Gibco, Thermo Fisher Scientific, Netherlands) and 2% B27 supplement (#17504/044; Gibco, Thermo Fisher Scientific, Netherlands) and cells were seeded on PEI-coated (polyethylenimine, #P3143) 8-well Ibidi plates (60 000 cells per well) or microfluidic devices (100 000 cells per plate, with one compartment seeded). Experiments were performed on day *in vitro* (DIV) 7–10.

Chemical compounds

Cells were treated with erastin to induce ferroptosis (catalogue number: 5449, Tocris) and ferrostatin-1 (Fer-1) to prevent it (catalogue number: SML0583, Sigma Aldrich). The mitochondrial calcium uniporter inhibitor (MCU-i4) was used to inhibit calcium uptake to mitochondria *via* the mitochondrial calcium uniporter (MCU) (Tocris; 7195). Human recombinant amyloid β protein fragment 1–42 ($Aβ_{1–42}$) was purchased from rPeptide, USA (catalogue number: A-1002-1 and catalog ID: A-1004-1). Stock solutions were prepared and dissolved following manufacturer's instructions. Corresponding volumes of the stock solutions were diluted in culture medium to reach the final concentrations listed, and the culture medium including the solvent was used as a vehicle.

Organelle staining and live cell imaging

For labelling mitochondria after erastin treatment, they were stained with VDAC (Product # PA1-954A, Thermo Fisher Scientific) at a dilution of 1 : 200 and imaged using a fluorescence Nikon Inverted Research Microscope ECLIPSE Ti2-E/Ti2-E.B. For imaging of mitochondrial movement, mitochondria were fluorescently labeled with 100 nM MitoTracker deep red (Invitrogen, Waltham, MA, USA). The cells were observed using a Zeiss Cell Discoverer 7 confocal laser scanning microscope, equipped with an Airyscan unit (Zeiss, Oberkochen, Germany), using a water immersion 50× objective (numerical aperture 1.2, magnification changer 1×). 672 × 672 pixel confocal images of the cells were recorded each 5 s for 7 min. The dye was excited with a 640 nm diode laser (far red) and detected through a quadruple band pass filter (425/30 + 514/30 + 592/25 + 709/100 nm). Temperature and CO_2 levels were kept constant during acquisition (37 °C, 5% CO_2).

Axonal mitochondrial tracking

Axonal mitochondria were tracked using the Fiji/ImageJ plugin TrackMate (version 7.12.1).[38–40] From each image, a region of interest was drawn to isolate one or a few mitochondria along the axons. Organelle trajectories were

automatically determined with the software and subsequently manually inspected to remove spurious points.[41]

Motion analysis

To characterize the motion of the mitochondria, the time-averaged mean square displacement was determined as previously described.[42] Briefly, for each trajectory, the displacement was calculated between all pairs of time points and subsequently averaged over all pairs of time points separated by the same time. The time-averaged mean square displacements of individual trajectories were subsequently also averaged over all the collected trajectories. The length of the collected trajectories differed as the axonal network is densely interconnected and thereby hampers the visualization of some of the mitochondria, some mitochondria move out of the field of view, and/or some mitochondria shift out of focus.

The motion was further characterized by determining the proportion of mitochondria that moved a certain threshold distance. To this end, the distance a mitochondrion moved from its starting position was determined as a function of time. A mitochondrion was considered to have moved if, at some point along its trajectory, it moved beyond the threshold.

Microfluidic chip fabrication

The two-compartment microfluidic chip model was previously established and we performed experiments using this model with slight modifications.[43] Briefly, the PFPE molds were made out of the PDMS axon-guidance chip master, fabricated using photo-and soft lithography.[44] The molds were filled with 1.5 g of the PDMS-prepolymer and curing agent mixture (10 : 1 wt ratio; Sylgard 184, Mavon B.V., Alphen aan de Rijn, Netherlands) and thermally cured to obtain the PDMS chips (dry oven, 1.5 h, at 70 °C). The PDMS chips were removed from the molds with a spatula and cut into squares using a scalpel. A dermal biopsy punch tool (Kai, 8 mm, F.V.D. Vooren B.V., Deventer, Netherlands) was used to open the reservoirs for media exchange. PDMS layer was adhered to glass coverslips (24 × 60 mm, Menzel Gläser) by oxygen plasma bonding at 310–320 mTorr for 20 s. The empty reservoirs were immediately filled with ultra-pure (UP) water, and the adherence of PDMS layer to the coverslip was boosted by placing the chips for 1 min at 70 °C on a heating plate, if necessary. The channels were sterilized by filling them with 70% ethanol for 20 min, RT, and washed 3 times with UP water. They were stored in sealed square plastic cell culture dishes (10.3 × 10.3 × 1.75 cm, Greiner bio-one) in a cold environment until further use. The evaporation of fluids from the chip was prevented by placing two circular culture dishes (10 × 35 mm, Greiner bio-one) filled with sterile UP water at the corners of the square plastic dishes. The final microfluidic axon-guidance device contained two parallel culture chambers connected by an array of microchannels, with four separate media reservoirs, each holding approximately 100 mm^3 of medium. Thanks to their position at the beginning and end of each cell compartment the neurons remained nourished. Finally, the neuron-on-a-chip model was established by differentiating the PCN in the microfluidic device for 6 days prior to exposure to various treatments.

Mitochondria movement imaging and analysis in the microfluidic chip

Mitochondria were labeled with 100 nM MitoTracker deep red and imaged right after an acute challenge with different treatments. For live cell imaging of motile mitochondria, the chips were imaged right after the addition of the treatment into the neuronal network compartment. We did not use the area of the microchannels for imaging because of the autofluorescence of the plastic microgrooves, which, after fluorescent labeling of mitochondria, interferes with visualizing the axons. Instead, we analyzed axonal fragments in the neuronal network compartment, with a minimal length of 12.2 μm, a maximal length of 403.7 μm, and an average length of 84.6 μm. Kymographs were generated using ImageJ (plugins-Kymograph-KymographBuilder), and we used KymoButler to help define and annotate the mitochondria movement, which were then manually checked and counted. In total, 51 axons from 6 independent microfluidic chambers were analyzed with the control-basal condition, 46 axons from 7 chambers with the erastin challenge, and 40 axons from 6 chambers with the ferrostatin-1 + erastin treatment. Concerning the amyloid-beta challenge experiment, we analysed 17 axons from 4 independent microfluidic chambers with the control-basal condition, 32 axons from 6 chambers with the amyloid-beta condition, and 18 axons from 5 chambers with the ferrostatin-1 + amyloid-beta treatment. Individual axonal measurements for each microfluidic chamber are reported in Fig. S1. Mitochondria were considered to be stationary if they did not move to the left or to the right throughout the acquired frames of the 7-minute time-lapse video. Motile mitochondria were those that moved towards somal compartment (anterograde) or neuronal network compartment (retrograde) during the acquired frames of the 7-minute long time-lapse video.

Mitochondria calcium imaging

A synthetic fluorescent mitochondria-targeted sensor was used for ratiometric imaging of mitochondrial calcium in live cells.[45] HT22 cells and PCNs were cultivated in 8-well ibidi plates at a density of 20 000 and 60 000 cells respectively. Loading mix was made by mixing 1 μL of 1 mM mt-Fura 2.3 AM and 1 μL of 20% Pluronic F-127 which was subsequently added to 1 mL of HBSS. Cells were washed with HBSS before applying 200 μL of loading mix to the wells and incubating them at 37 °C and 5.0% CO_2 for 15 minutes. The cells were washed once more with HBSS before imaging.

The cells were imaged with a Nikon Fluorescent microscope, using excitation wavelengths of 340 nm (fura340, a green laser at 30%), which measures the calcium-bound mt-Fura 2.3, and 380 nm (fura380, a blue laser at 7%), which

measures free mt-Fura 2.3 AM. The ratio between the two wavelengths was determined using the formula below. Thus, an increased ratio represents an increase in mitochondrial calcium, whereas a decreased ratio represents an increase in mitochondrial calcium. Depending on the cell type, time measurements of 5 or 15 minutes were made, imaging every 1 second and measuring the ratio of fura340/fura380. HT22 cells were imaged for 5 minutes, whereas PCN were imaged for 15 minutes, of which the first 2 minutes were used to determine the baseline. The imaging time for PCN was prolonged compared to experiments performed in HT22 cells to investigate long-term effects on mitochondrial calcium. The results were analyzed by selecting 20 cells at random, creating regions of interest (ROIs), using a bezier tool (Fig. S2). The ratio of fura340/fura380 was measured while correcting for the background fluorescence. The generated values were used to create graphs corresponding to each separate ROI.

Microelectrode array (MEA)

Primary cortical neurons (PCNs) were seeded on a 0.5% w/v polyethyleneimine (PEI)-coated MEA plate (Axion Biosystems, United Kingdom, M768-tMEA-48 W) at a density of 1.2×10^5 cells per well, in medium containing 10 μg mL^{-1} laminin. A 5 μL cell suspension was placed in the center of each well and incubated for 1 hour, followed by the addition of neurobasal medium. MEA recordings of PCNs were conducted using the Maestro multi-well MEA system (Axion Biosystems, USA). The MEA plate was inserted into the Maestro system (37 °C, 5% CO2), and spike detection and neuronal electrical activity were assessed on day 14 (DIV 14) with treatment with Aβ and various compounds. Neuronal spikes were recorded using Axion AxIS software for firing rate analysis.

Statistical analysis

Statistical significance was evaluated using an unpaired Student's *t*-test or ANOVA followed by Tukey's *post hoc* test for multiple comparisons. Data analysis was performed with GraphPad Prism software (version 8.0, GraphPad Software Inc., La Jolla, CA, USA). Measurements of the mitochondrial movement in either antero- or retro-grade direction (represented as percentage of total mitochondria/axon) were performed in neuronal axons. All traceable axons were examined in each microfluidic chamber. Minimum of 3 microfluidic devices were included in the analysis, containing primary neurons derived from at least three independent neuronal cultivations. For the results from mitochondrial calcium imaging, the distribution of the generated values was determined using a Shapiro–Wilk normality analysis. Statistical significance between three time points-baseline, after adding the treatment, and at the end of the measurement-was determined using a repeated measures one-way ANOVA with a Geisser–Greenhouse correction when the values were normally distributed. When the values were not normally distributed, a nonparametric Friedman test was conducted. Statistical significance in the area under the curve between two treatments was determined using a Mann–Whitney test. Results were expressed as mean ± SD for all experiments. Differences were considered significant when the p value was lower than 0.05 ($*p < 0.05$, $**p < 0.01$, $***p < 0.001$, $****p < 0.0001$).

Results

The mitochondrial movement in neurons is heterogeneous

To investigate mitochondrial dynamics in neuronal cells and quantify the proportion of static *versus* moving mitochondria, we used PCNs and mitochondria fluorescently labelled with MitoTracker deep red dye. Mitochondrial dynamics was analyzed by confocal microscopy every 5 s for 7 min for a total of 85 frames (Fig. 1A). The trajectories traced by the mitochondria were next determined (Fig. 1B) for further analysis. Qualitative inspection showed that the mitochondria exhibited highly heterogeneous motion, both considering a single mitochondrion over time, as well as comparing different mitochondria (Fig. 1B). Some mitochondria moved large distances rapidly (Fig. 1B, trajectory 1), while other mitochondria remained stationary for an extended period of time before moving (Fig. 1B, trajectory 3), and others yet remained fairly stationary throughout the observation time (Fig. 1B, trajectory 2). For a more quantitative analysis, we acquired multiple fields of view and tracked all mitochondria located in axons, resulting in 62 individual trajectories (Fig. 1C).

Most of the observed mitochondria exhibited limited displacement. Using a threshold of 2 μm, approximately ten times the average mitochondrial diameter observed in this study, the majority of mitochondria remained within this range, indicating limited movement (Fig. 1D). Using other threshold distances indicate that the smaller the threshold is, the bigger the percentage of motile mitochondria (Fig. S3).

For a more detailed analysis of how far the mitochondria move, we determined the mean square displacement of individual mitochondria as a function of time. The mean was calculated over time, meaning that instead of simply measuring how far a mitochondrion moved in the first 5 seconds of recording, we averaged the distance covered across all its 5-second intervals. Furthermore, the displacement was squared, because the average displacement is (typically) 0, as the object moves back and forth. The mean square displacement as a function of time of 10 random mitochondria show that most mitochondria do not move that far for the first 5–10 s of the observation time, but at longer timescales they start moving further (Fig. 1E). These results also illustrated how heterogeneous the motion is, with individual mitochondria exhibiting quite different mean square displacements compared to others. To get a better idea of the general behavior we subsequently averaged the mean square displacement over all trajectories, resulting in a smooth curve (Fig. 1F). This mean square displacement increased roughly linearly (in log scale) as a function of time

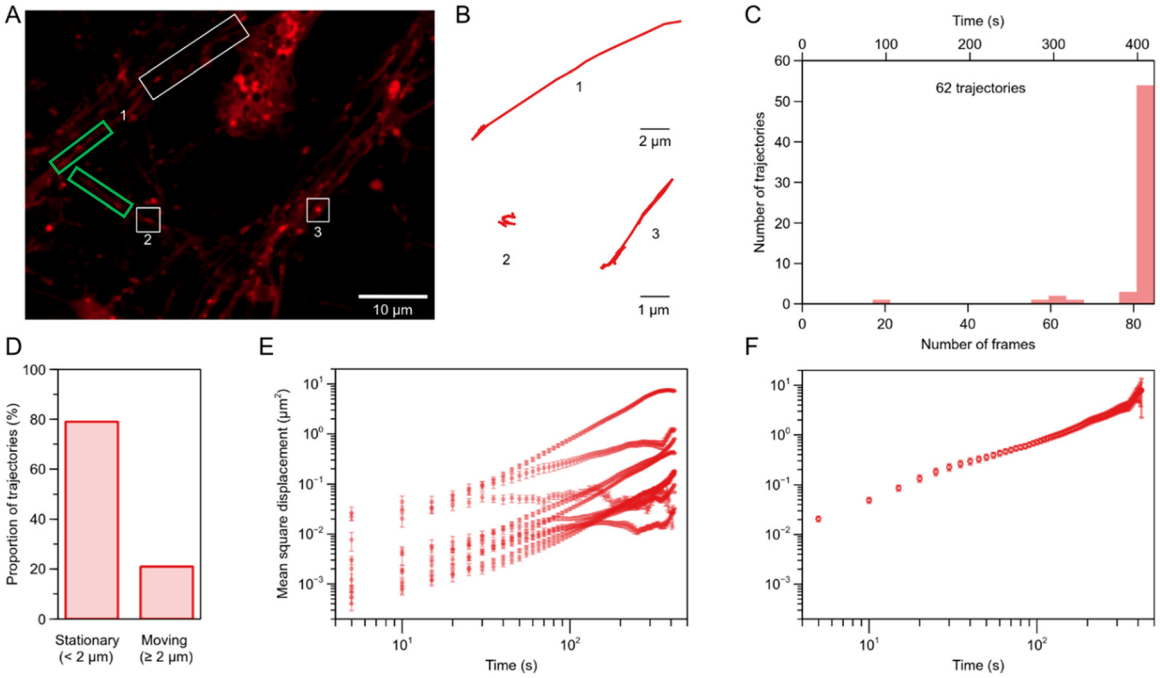

Fig. 1 Mitochondrial motion analysis in primary neurons. (A and B) Collection of mitochondrial trajectories. Imaging of primary neurons was used to track mitochondria within axons (A), and their corresponding trajectories (B) were analyzed. (Green rectangles) Axon segments. (White rectangles) Three example of mitochondria whose trajectories are shown enlarged in panel B. (C) Mitochondrial trajectory length distribution as a function of number of frames (lower *x* axis) and time (upper *x* axis). In total 62 trajectories were collected. (D) Proportion of mitochondria considered as moving or stationary based on a 2 μm threshold. (E and F) Time-averaged mean square displacement of 10 randomly chosen mitochondria trajectories (E) and further averaged over all collected trajectories (F). Error bars in E and F represent standard error of the mean. For most of the data points, the error is very small, resulting in error bars that are smaller than the symbol size and therefore not visually discernible. Note the log-scale on both axes.

up to around 30–40 s, after which there was a slight change of slope lasting until the end of the observation time.

Overall, this general characterization of how the mitochondria move in neuronal protrusions showed that mitochondria move in a highly heterogeneous fashion and that most mitochondria do not move very far. Our results are consistent with a previous finding showing that the majority of mitochondria in axons move heterogeneously, with long durations of stalling.[46] While we can thus analyze how the mitochondria move in a neuronal network, closer to their native state, this approach nevertheless does not allow us to discriminate the directionality of the motion, which is affected in disease-related state.

Isolation of neuronal network and mitochondrial labelling on a microfluidic chip

In order to track mitochondrial movement along axons and discriminate the directionality of the motion, we established a microfluidic chip model by seeding PCNs in the somal compartment on the chip. The seeded cells included a co-culture of astrocytes and neurons isolated from the mouse cortex (Fig. 2A). After differentiating the PCNs for a week, a mature neuronal network formed (Fig. 2B), which allowed us to visualize mitochondria in the axons of live cells (Fig. 2C). To see whether ferroptosis induction has an effect on the neuronal network, we treated the somal compartment of the microfluidic chip with the ferroptosis inducer erastin (50 μM) (Fig. 2D).[47] After 24 hours, no mitochondria were able to be visualized because of the disruption of neuronal network. This was prevented by Fer-1 pretreatment for 1 hour (1 μM) (Fig. 2E). Altogether, these results suggest that initiation of ferroptosis with erastin caused disruption of the neuronal network and that by using a two-compartment microfluidic chip allows for tracking anterograde and retrograde movement of mitochondria in isolated axons of PCNs.

An acute challenge with Aβ increased retrograde and decreased anterograde movement of mitochondria, which can be prevented by Fer-1

Next, we investigated the effects of the acute challenge with an ferroptosis inducer on mitochondrial dynamics in neuronal cells. The precisely designed openings (15 μm on the somal side and 3 μm on the axonal side) and the funnel shape of the microchannels of the microfluidic device allowed us to determine the motility and the direction of the mitochondrial movement. Mitochondria going from the somal to neuronal network compartment moved in the anterograde direction and mitochondria going form the neuronal network to somal compartment moved in the

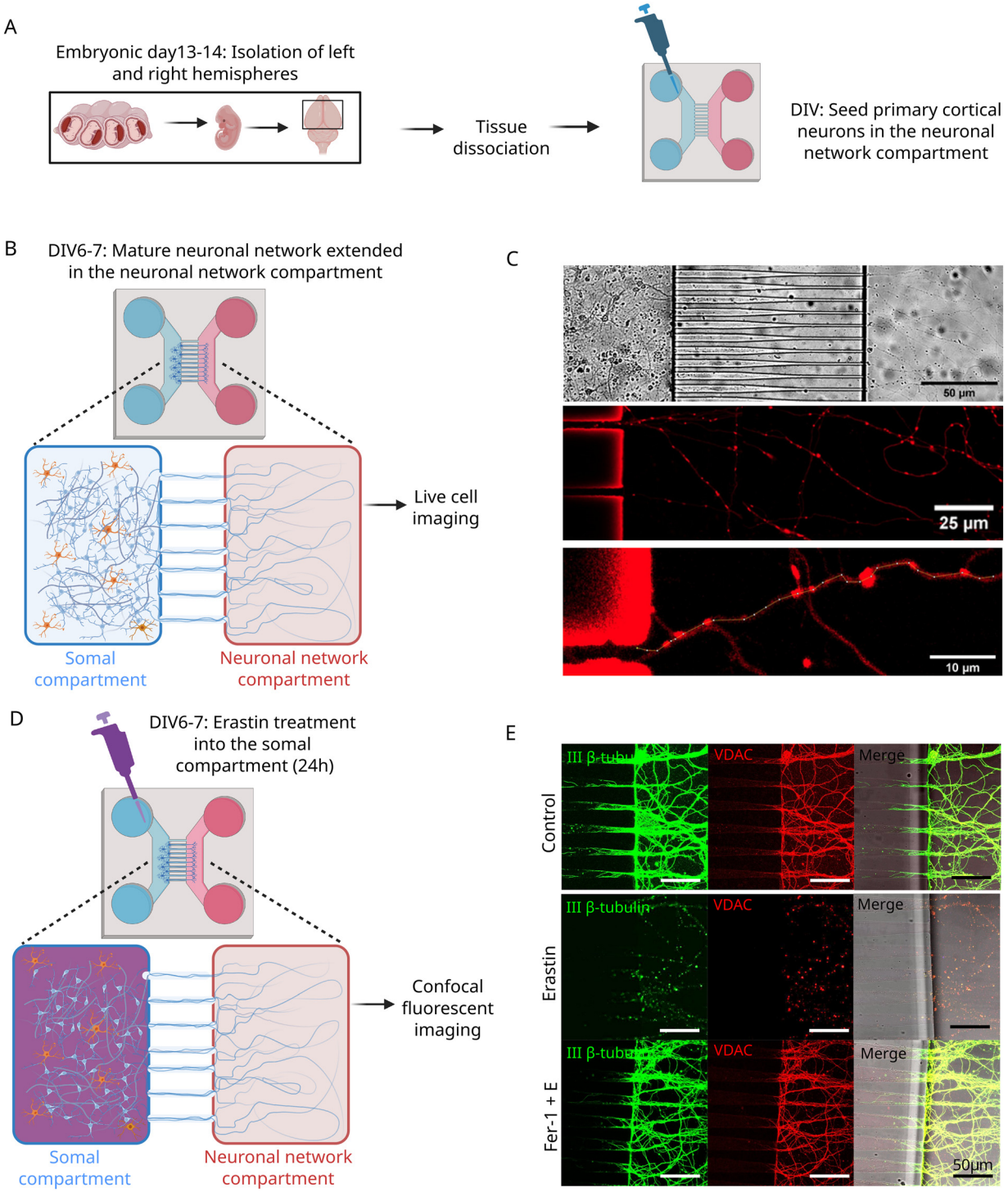

Fig. 2 Establishing the brain-on-a-chip model to track anterograde and retrograde mitochondrial movement. (A) Experimental design for PCNs isolation and seeding. (B) Schematic diagram of the microfluidic device. Neuronal cell body compartment (somal compartment), and neuronal network (axon) compartment. The compartments are connected *via* microchannels (450 µm long, 15 µm wide opening in soma and 3 µm wide opening in the axon compartment), constructed in a funnel shape allowing only dendrites/axons to pass from somal to neuronal network compartment, which is devoid of neuronal cell bodies as no DAPI can be detected. PCNs were seeded into the somal compartment of the microfluidic device with a density of 100 000 cells. On DIV 6–7, the neuronal network reached and extended into the adjacent compartment *via* microchannels. (C) Representative brightfield photo of PCNs on DIV6 in microfluidic device (top), and fluorescent images of the neuronal network compartment depicting PCNs labelled with MitoTracker deep red (middle and bottom with scale bars 25 µm and 10 µm respectively). (D) Schematic diagram of the experimental design for ferroptosis induction to PCNs in the microfluidic device. PCNs were treated in the somal compartment with erastin 30 µM for 24 h. (E) Representative images of neuronal network compartment of the microfluidic device after ferroptosis induction with erastin and co-treatment with Fer-1 which resulted in protection against ferroptosis-induced loss of neuronal network (β 3 tubulin staining the neuronal network in green on the left, VDAC staining mitochondria in red in the middle, and overlay images on the right). The A, B and D parts of this figure were generated using BioRender.

retrograde direction. To illustrate how mitochondrial directionality was analyzed and to visually appreciate the underlying motility patterns, a representative time-lapse recording of axonal mitochondria under the indicated treatment conditions is included (Video S1). To determine whether the disruption of mitochondrial movement, linked to neurodegeneration and aging,[48–50] can be mimicked by a ferroptosis inducer, we evaluated the proportions of stationary and motile mitochondria during an acute challenge with erastin. Among the motile mitochondria, we further assessed the percentages of anterograde *versus* retrograde movement following various acute challenges (Fig. 3). Adding media or solvent control media to the neuronal network compartment had no effect on neither the percentage of stationary *vs.* motile mitochondria nor on the direction of mitochondrial movement (Fig. 3A and B).

To mimic a pathological feature of neurodegeneration, we challenged neurons with $A\beta_{1-42}$. To model the initial phases of neuronal degeneration and an early stage of neurodegenerative pathology, we specifically treated the axonal/network compartment, where axon terminals reside, rather than the somal compartment, reflecting the principle that neuronal network alterations occur before overt somatic cell death in Alzheimer's disease.

We treated the neuronal network compartment of the microfluidic device with acute challenges of slightly lower concentration of erastin (30 μM) in order not to induce cell death but to increased ferroptosis vulnerability in the cells, or to mimic AD pathology with $A\beta_{1-42}$ (5 μM). In order to investigate whether ferroptosis pathway is involved in the potential alteration of the mitochondrial motility as a response to erastin or $A\beta_{1-42}$ challenge, we used a lipid peroxidation inhibitor, Fer-1 (1 μM).[51] Fer-1 was incubated either 1 hour before the additional ferroptotic challenge or as a co-treatment (Fig. 3C).

We visualized the movement using analysis of kymographs, that plot space (horizontal) over time (vertical) and tracked the mitochondria movement using KymoButler program (Fig. 3C). Ferroptosis induction had no effect on the percentage of stationary *versus* motile mitochondria (Fig. 3E) but significantly decreased the percentage of mitochondria moving anterograde (from somal to the neuronal network compartment) and increased those moving in the retrograde direction (from axonal terminals back to the soma) (Fig. 3F). Pretreatment with Fer-1 prevented against the effects on mitochondrial directionality induced by erastin (Fig. 3F). Similarly, addition of $A\beta_{1-42}$ had no effect on the percentage of stationary *vs.* motile mitochondria (Fig. 3G). Aβ-related challenges resulted in significantly lower anterograde and higher retrograde mitochondrial movement, which was also prevented by pretreatment with Fer-1 (Fig. 3H). Altogether these results indicate that Aβ alters directionality of mitochondria movement in axons and dendrites, which can be rescued by Fer-1 treatment.

To address the potential link between mitochondrial movement and mitochondrial calcium in ferroptosis in neuronal cells, we employed an optimized version of the recently developed mitochondria-targeted mt-Fura 2 Ca^{2+} probe, mt-Fura-2.3 AM (45). Mt-Fura-2.3 AM contains a positively charged triphenylphosphonium (TPP) group that allows its accumulation in the negatively charged mitochondrial matrix. The increase in the 340/380 nm excitation ratio translates to increase in mitochondrial calcium. We evaluated whether ferroptosis vulnerability and Aβ-related effects on mitochondrial movement are associated with disruption of mitochondrial calcium. To optimize the measurements of mitochondrial calcium in neuronal cells, we first tested whether mt-Fura-2.3 AM co-localizes with a mitochondrial marker, MitoTracker red in a neuronal-like cell line, HT22 cells, and in primary neurons (Fig. 4A).

Based on the co-localization results, we concluded that mt-Fura-2.3 AM is able to accumulate in mitochondria of HT22 cells. Measurements of mt-Fura-2.3 AM in un-treated HT22 cells, revealed a slight increase in the 340/380 nm excitation ratio, indicating a small rise in mitochondrial calcium (Fig. S4A–C). After addition of HBSS media, the slight increase in mitochondrial calcium was observed being similarly to the baseline measurement (Fig. S4D–F). However, upon addition of KCl (100 mM), a large increase in mitochondrial calcium could be observed ($p < 0.0001$), which also stayed elevated for the duration of the measurements ($p < 0.0001$) (Fig. S4G–I).

We next tested whether mt-Fura-2.3 AM localises in the mitochondria in PCNs by co-staining the cells with mt-Fura-2.3 AM and MitoTracker red (Fig. 4B). Similarly, as shown in HT22 cells, based on the observation that mt-Fura 2 AM co-localises with MitoTracker deep red in cortical neurons as well, we concluded that mt-Fura-2.3 AM will provide information about mitochondrial calcium in PCNs.

We then visualized calcium-bound mt-Fura-2.3 AM by excitation at 340 nm, as well as free mt-Fura-2.3 AM by excitation at 380 nm, analyzing the 340/380 nm excitation ratio as an indicator of mitochondrial calcium (Fig. 4C). No significant differences in mitochondrial calcium were detected following addition of the HBSS media or solvent media ($p > 0.9999$) (Fig. 4D–F). This led us to conclude that any effects observed in the following experiments were due to the treatment, not due to the addition of medium or solvent. Several calcium oscillations could be detected during the measurements, which could be attributed to physiological neuronal firing, indicating that neuronal firing activity can influence mitochondrial calcium.[52–55] Application of KCl (100 mM) to primary neurons led to an immediate response followed by a strong increase in mitochondrial calcium ($p < 0.0001$), which stayed elevated for the duration of the measurement ($p < 0.0001$) (Fig. 4G–I). After addition of ATP (100 μM), an immediate, short-term increase in mitochondrial calcium was observed ($p < 0.0001$) (Fig. 4J–L). This effect is in line with previous research, where a peak was detected in response to ATP application.[56–58] Our findings indicate that mt-Fura-2.3 AM is a suitable dye to observe alterations in mitochondrial calcium in primary

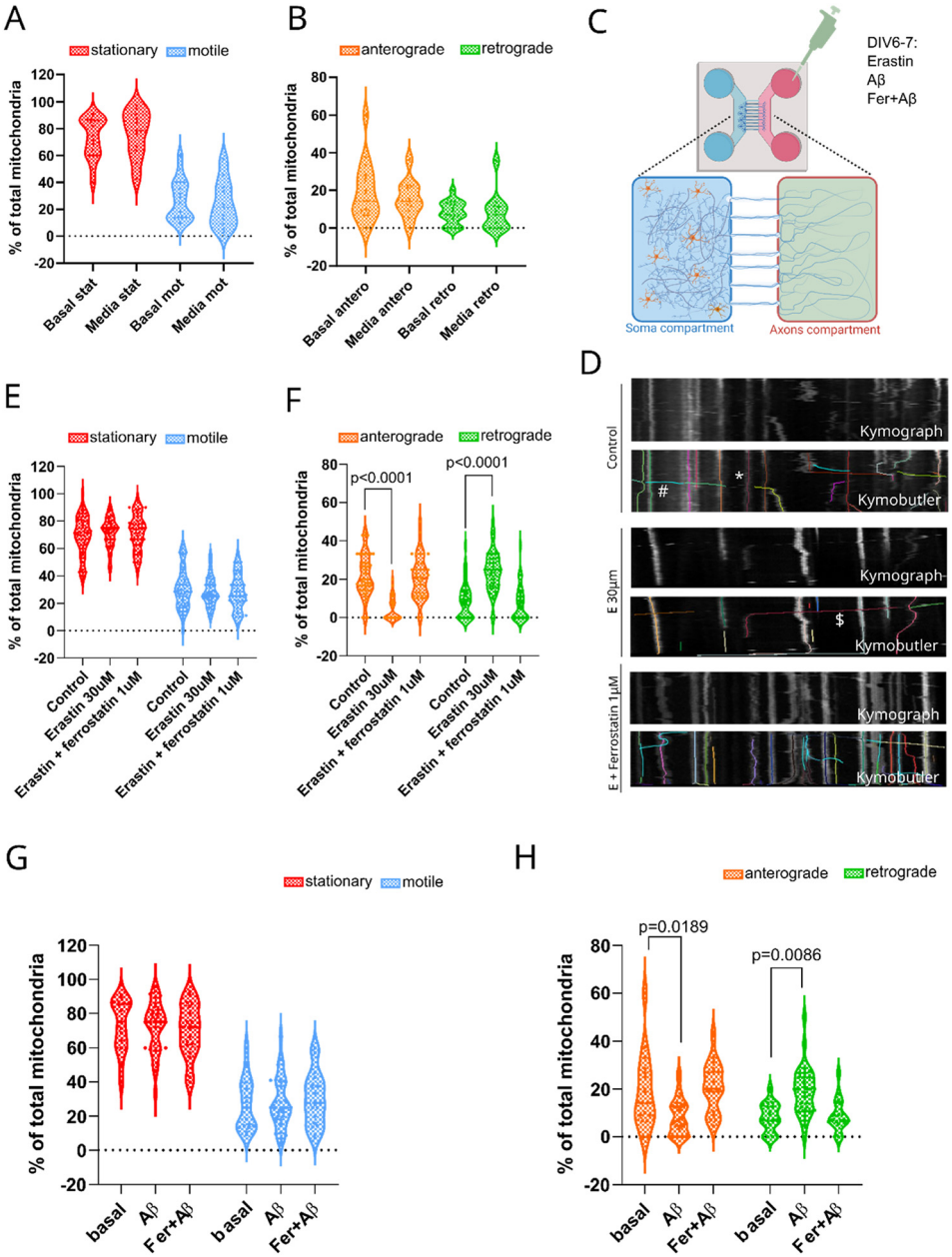

Fig. 3 Erastin and $A\beta_{1-42}$ decrease anterograde mitochondrial movement in PCNs. (A) Percentage of stationery and motile mitochondria. Approximately 85% of mitochondria were stationery and 15% mitochondria were motile. After addition of media to the neuronal network compartment the % of stationary and motile mitochondria did not change upon addition of media compared to the basal condition (recording before addition of media). Between 11 and 17 axons were tracked per condition. (B) Percentage of anterograde and retrograde mitochondria. Approximately 20% of total mitochondria were anterograde and 10% mitochondria were retrograde. After addition of media to the neuronal network (axonal) compartment the % of both anterograde and retrograde mitochondria did not change upon addition of media compared to the basal condition (recording before addition of media). Between 11 and 17 axons were tracked per condition. (C) Experimental design of treatment PCNs with ferroptosis and Aβ challenge to the neuronal network on the microfluidic chip. (D) Examples of generated kymographs used for mitochondrial movement tracking in single axons (top) treated with erastin 30 μM and Fer-1 1 μM and tracking mitochondria with kymobutler (bottom). Vertical lines represent stationary mitochondria (≅* symbol depicts stationary mitochondria), and horizontal lines represent motile mitochondria (symbol depicts anterograde, $ depicts retrograde movement). (E) Percentage of stationary and motile mitochondria was not affected by acute ferroptosis challenge with erastin or a combination of erastin (30 μM) and Fer-1 (1 μM). Between 40 and 51 axons were tracked per condition. (F) Erastin induced significantly lower percentage of anterograde and significantly higher retrograde ($p < 0.0001$) mitochondria which was prevented by Fer-1 co-treatment. Between 40–51 axons were tracked per condition. (G and H) Similar effect showing no alteration of the percentage of motile *vs.* stationary mitochondria and decreased anterograde (p = 0.0189) and increased retrograde (p = 0.0086) of mitochondria was observed with acute challenge with $A\beta_{1-42}$ (5 μM). Co-treatment with Fer-1 (1 μM) prevented the Aβ-related changes on mitochondrial movement. Between 11 and 17 axons were tracked per condition. In graphs A, B, E, F, G, and H each data-point represents the percentage of mitochondria moving in anterograde or retrograde direction in an individual axon. All traceable axons were analyzed in each microfluidic chamber. The data contains values from at least three separate microfluidic devices, containing neurons derived from at least three independent primary neuronal cultivations. Statistical significance was determined using one-way Anova. Part C of this figure was generated using BioRender.

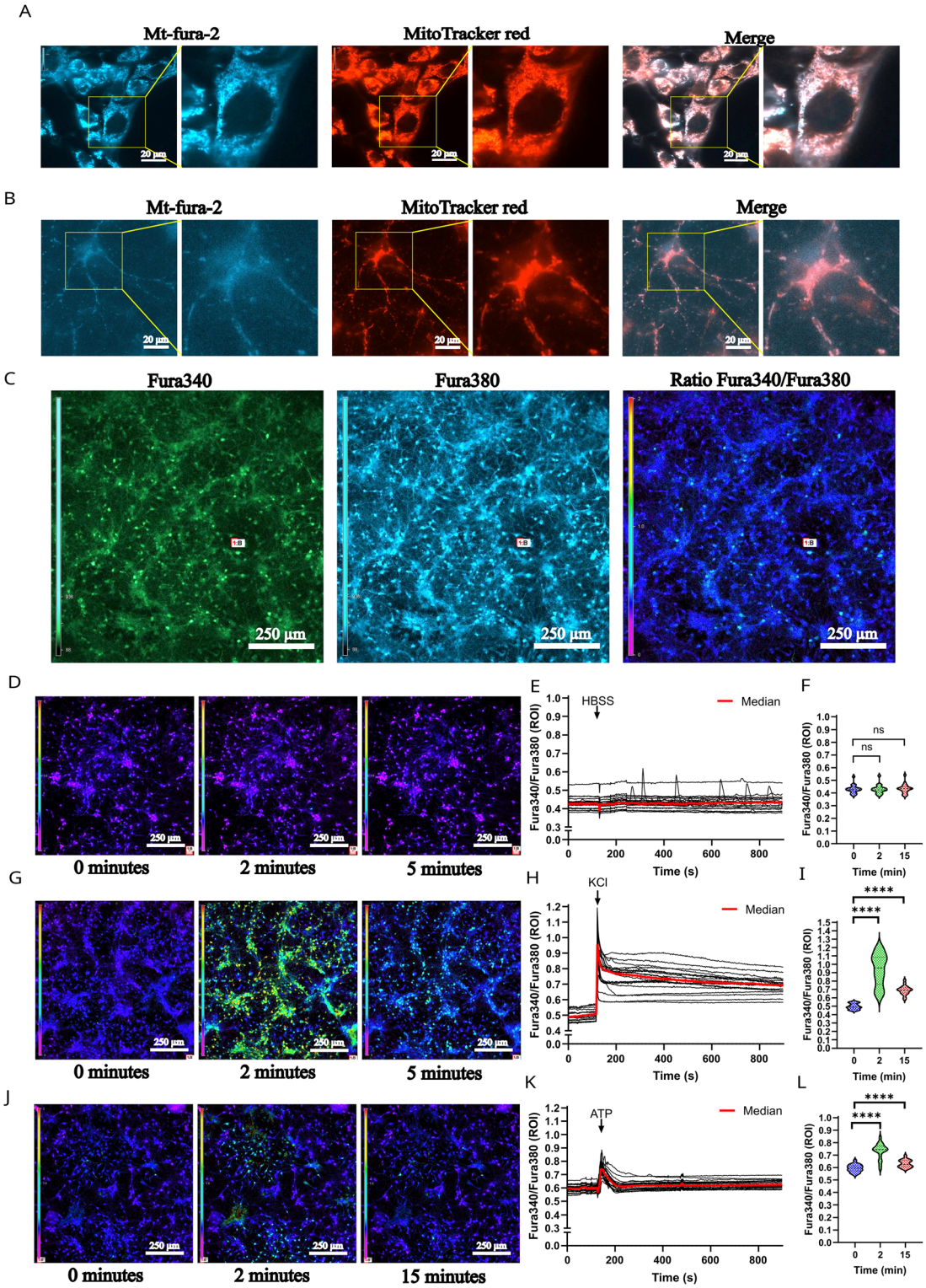

Fig. 4 Mitochondrial calcium imaging using mt-Fura-2.3 AM in HT22 cells and cortical neurons. (A) HT22 were loaded with mt-Fura-2.3 AM and incubated with MitoTracker red. Images were acquired at 60× magnification and imaged at 380 nm and merged image was created. (B) Primary cortical neurons (PCNs) were loaded with mt-Fura-2.3 AM and incubated with MitoTracker red. Images were acquired at 60× magnification and imaged at 380 nm and merge image was created. (C) PCN loaded with mt-Fura-2.3 AM and imaged at 340 nm (left), at 380 nm (center) and calculated ratio of excitation 340/380 nm (right) is visualized at 20× magnification. (D–J) The ratio of 340/380 nm was analyzed following addition of HBSS media, KCl (100 mM) and ATP (100 μM) in PCNs. (D, G and J) Representative capture images show the ratio images collected at the baseline (depicted as 0 minutes), at the addition of various compounds (depicted as 2 minutes) and at the end of the experiment (depicted as 15 minutes). (E, H and K) Each graph represents 20 imaging traces that correspond to 20 neuronal cells, chosen at random. The average of these calcium traces are shown as a thick red line. (F, I and L) The quantification of the mitochondrial calcium traces shows the effect of HBSS (n = 9), KCl (100 mM, n = 7) and ATP (100 μM, n = 3) on PCNs. Statistical significance was determined by one-way Anova (****$p < 0.0001$).

neurons, as mitochondrial calcium increased in response to classical calcium inducers, ATP and KCl.

Inhibition of ferroptosis prevents increases in mitochondrial calcium mediated by $A\beta_{1-42}$

To evaluate whether the Aβ-related effects on mitochondrial movement can be also linked to changes in mitochondrial calcium, we treated PCNs with $A\beta_{1-42}$ and measured changes in mitochondrial calcium using mt-Fura-2.3 AM. Interestingly, $A\beta_{1-42}$ caused an initial increase in mitochondrial calcium, followed by mitochondrial calcium oscillations ($p < 0.0001$) (Fig. 5A). Pretreatment with Fer-1 (1 μM) for 1 hour before the addition of $A\beta_{1-42}$ (5 μM) rescued the Aβ-related mitochondrial calcium increase ($p < 0.0001$) (Fig. 5B) compared to $A\beta_{1-42}$ alone, also less mitochondrial calcium oscillations were observed.

To test whether the effects of $A\beta_{1-42}$ measured with mt-Fura 2 AM are mediated *via* mitochondrial calcium uniporter and related to mitochondrial calcium signaling, we pre-treated the neurons with an inhibitor of MCU, MCU-i4,[25,59,95] and then challenged the cells with $A\beta_{1-42}$. The pre-treatment with MCU-i4 (1 μM) reduced the mitochondrial calcium increase caused by $A\beta_{1-42}$ ($p < 0.0001$) (Fig. 5C). The analysis of the number of peaks and the area under the curve (AUC) in the last 10 minutes of the normalized results after addition of $A\beta_{1-42}$ to Fer-1 and MCU-i4-pretreated cells revealed no change in the number of peaks (Fig. 5D). However, both Fer-1 and negative modulation of the MCU resulted in a significantly lower AUC compared to Aβ alone ($p = 0.0001$ and $p < 0.0001$ respectively) (Fig. 5E). Altogether our data suggest that Aβ-induced mitochondrial calcium deregulation could be associated with ferroptosis pathway, as it can be mitigated by pre-treatment with Fer-1 in cortical neurons.

The Aβ-related effects on mitochondrial movement and mitochondrial calcium are associated with increased neuronal activity in cortical neurons

We recorded neuronal activity using MEA measurements, as previously described.[36] To assess the effect of $A\beta_{1-42}$ on action potential (AP) firing and its modulation by Fer-1 and MCU-i4, we measured spontaneous activity of PCNs in 48-well MEA plates after treatment with $A\beta_{1-42}$ (Fig. 6). $A\beta_{1-42}$ (5 μM) increased firing rates 45 min post-treatment (0.44 ± 0.16 Hz) compared to its untreated control (0.38 ± 0.13 Hz) as shown in the spiking map, confirming $A\beta_{1-42}$-induced hyperactivity (Fig. 6A and B).

Pre-treatment with Fer-1 (1 μM) for 1 h did not prevent this $A\beta_{1-42}$-triggered neuronal burst activity, while pre-treatment with MCU-i4 (1 μM) for 1 h slightly reduced firing rates (Fig. 6C and S5). These results suggest that $A\beta_{1-42}$-induced hyperactivity can be attenuated by inhibiting mitochondrial calcium uniporter complex, but not by lipid peroxidation inhibition with Fer-1.

Discussion

In this study, we revealed that acute challenge with $A\beta_{1-42}$ is linked to increased retrograde *vs.* anterograde movement of axonal mitochondria, deregulation of mitochondrial calcium and increased neuronal activity in PCNs. Based on previous work in primary cortical neurons showing that erastin increases ROS and that ferrostatin-1 suppresses lipid peroxidation, we used ferrostatin-1 as a pharmacological tool to probe the involvement of ferroptosis-related oxidative stress.[60–62] Pre-treatment with an inhibitor of lipid peroxidation, Fer-1 protected against mitochondrial movement and calcium homeostasis-related effects but did not mitigate alterations in neuronal activity. These findings suggest that targeting the oxidative stress component of the ferroptosis pathway could help alleviate AD-related disruptions in mitochondrial function and calcium signaling.

The mitochondrial movement analysis revealed that primary cortical neurons show a very heterogeneous dynamics in time, with most mitochondria displaying long moment of stalling and a smaller proportion performing unidirectional motion (for 2 μm or longer). This is in accordance with previous literature about mitochondrial movement, showing the complex nature of this process and its importance for correct neuronal functioning.[46,63–66] It has been shown that retrograde signaling is essential for maintaining neuronal health.[26,27,67] We found that following an acute challenge with erastin or $A\beta_{1-42}$, neurons increase their retrograde mitochondrial movement, which could be a potential protective mechanism to boost neuronal health.[27] Literature suggests that axonal transport disruption is a key feature of neurodegeneration.[68] Additionally, we provided a link to ferroptosis since Fer-1 protected against the disrupted mitochondrial movement induced by $A\beta_{1-42}$. Compromised anterograde mitochondrial transport in chronic glaucoma optic nerve explants has been observed, when compared to control explants.[69] Similar to other neurodegenerative diseases such as AD and Parkinson's disease (PD), glaucoma involves mechanisms such as mitochondrial dysfunction, oxidative stress ad impaired axonal transport. This aligns with our observation of decreased anterograde transport following an acute erastin or $A\beta_{1-42}$ insult. Overexpression of P301L tau in primary cortical neurons decreased anterograde transport while sustaining retrograde movement, reducing axonal mitochondrial density due to decreased kinesin recruitment, as determined by immunoblotting.[70]

The mitochondrial calcium increase followed by increased oscillations induced by $A\beta_{1-42}$ was prevented by Fer-1 pretreatment. It is known that $A\beta_{1-42}$ can cause an increase in calcium in the cytosol by formation of pores[22] and by calcium release from the ER through the activation of the RyRs, leading to fluctuations of calcium levels.[18,23,24] Due to the buffering role of mitochondria, it can be reasoned that the increase in calcium, as well as the fluctuations, could also be detected in the mitochondrial matrix.[71] According to Sakamuri *et al.*, addition of $A\beta_{1-42}$ has a negative effect on

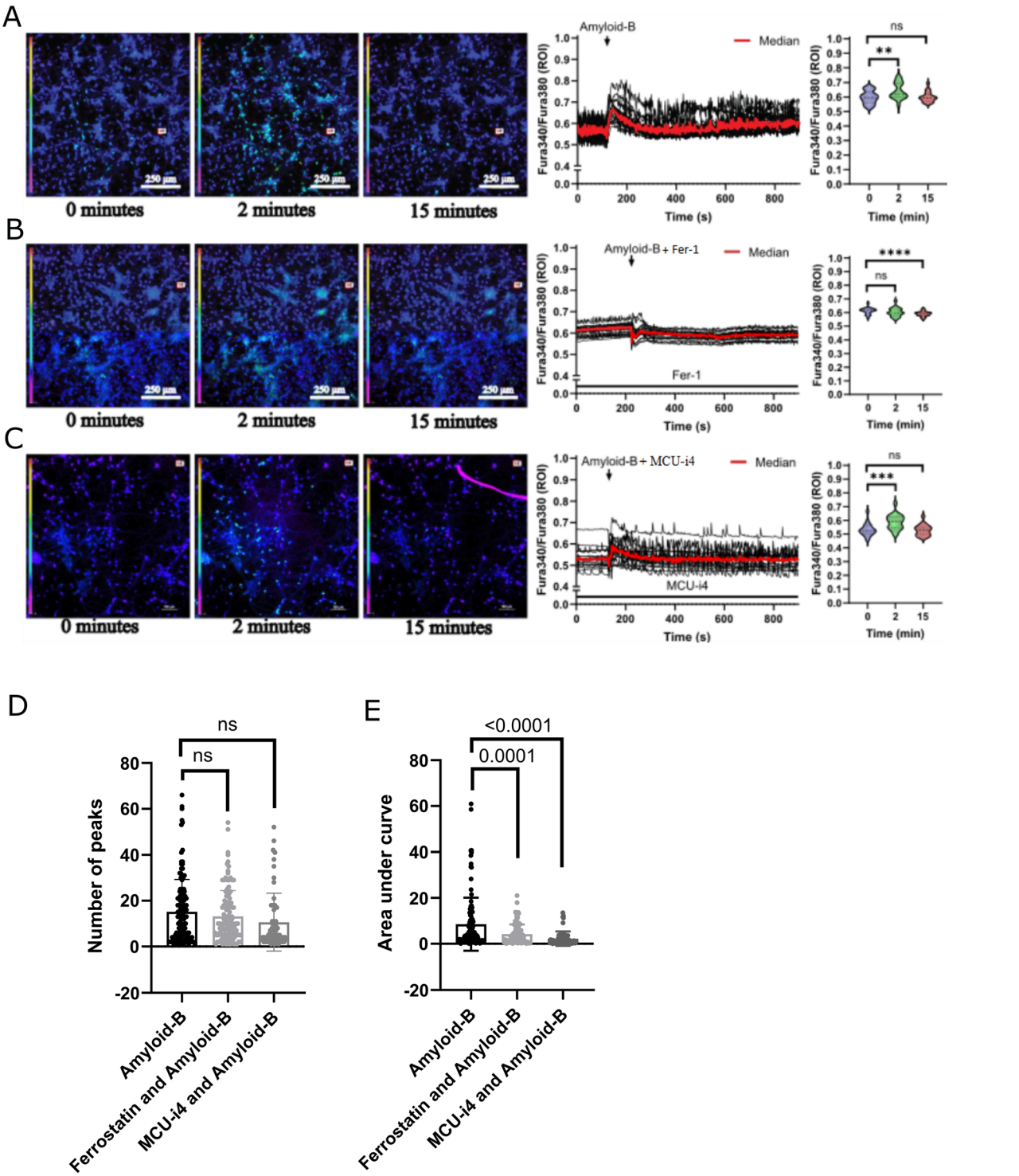

Fig. 5 $A\beta_{1-42}$ increases mitochondrial calcium that can be prevented by ferrostain-1 (Fer-1) and mitochondrial calcium uniporter inhibitor (MCU-i4) (A–C) The ratio of fura340/fura380 was measured in PCNs after addition of $A\beta_{1-42}$. 3 captures are shown from left to right during imaging at the baseline, directly after addition of treatment and at the end of imaging. Each graph represents 20 cells, chosen at random. The median is shown as red line. Area under curves (AUC) were determined from the last 10 minutes of experiments, calculated from normalized graphs. (A) Shows the addition of 5 μM $A\beta_{1-42}$ which caused an initial increase in mitochondrial calcium, followed by mitochondrial calcium oscillations ($p < 0.0001$) ($n = 7$). (B) Shows addition of 5 μM Aβ to PCN that were pretreated with 1 μM Fer-1 for 1 hour before the addition of $A\beta_{1-42}$ (5 μM) which rescued the Aβ-related mitochondrial calcium increase ($p < 0.0001$) ($n = 5$). (C) Shows addition of 5 μM $A\beta_{1-42}$ to PCN that were pretreated with 1 μM mitochondrial calcium uniporter inhibitor (MCU-i4) for 1 hour reduced the mitochondrial calcium increase caused by $A\beta_{1-42}$ ($p < 0.0001$) ($n = 3$). (D) Number of peaks and (E) AUC of Aβ treated, and Fer-1 and MCU-i4 pretreated cells from 1 representative experiment ($n = 3$ independent experiments). While there was no change in number of peaks, both ferroptosis inhibition with Fer-1 and negative modulation of the MCU resulted in a significantly lower AUC compared to $A\beta_{1-42}$ alone ($p < 0.0001$) ($n = 3$ independent experiments). The statistical significance was determined using one-way Anova (***$p < 0$, 001, ****$p < 0.0001$).

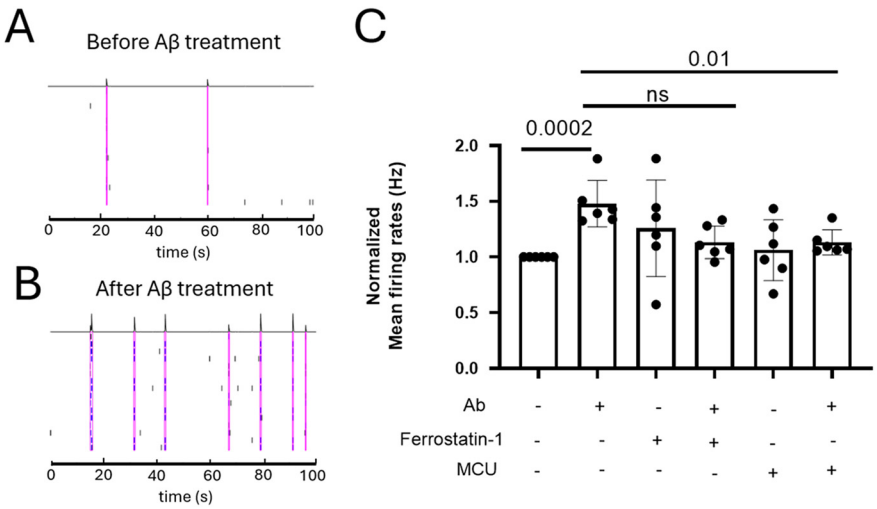

Fig. 6 $A\beta_{1-42}$ increases neuronal activity in cortical neurons. (A and B) Spontaneous activity of neurons in the medium with and without extracellular $A\beta_{1-42}$. Amyloid induces increased neuronal activity. (C) Normalized mean firing rates were measured in the presence and absence of $A\beta_{1-42}$, with Fer-1 and MCU treatments. The spiking rate increased significantly in the presence of $A\beta_{1-42}$. MCU-i4 significantly reduced the $A\beta_{1-42}$-induced firing rate, whereas Fer-1 had no effect. Data are presented as mean ± SD, and statistical difference was calculated with an unpaired *t*-test. Independent experiments were repeated 3 times.

OXPHOS and ATP production.[72] On the other hand, other studies have found hyper-metabolism, by increased OXPHOS, as a result of $A\beta_{1-42}$ treatment.[73,74] Various sources affirm the effect of $A\beta_{1-42}$ on cytosolic calcium.[18,22,75,76] Calvo-Rodriquez *et al.* use Fura-2 AM as cytosolic calcium probe and found that $A\beta_{1-42}$ elicits an immediate increase in cytosolic calcium, which was paralleled by the increase in the mitochondrial calcium,[77] as observed in the current study. Specific to mitochondria, Shevtsova *et al.* revealed an increase in mitochondrial calcium after addition of $A\beta_{1-42}$, although it was not as immediate as observed in our experiments.[76] However, this could be attributed to a different mitochondrial calcium probe, x-rhod-1AM, its potential ability to affect mitochondrial structure, and to lower concentration of $A\beta_{1-42}$ used.[76,78] We recognize that the 5 μM concentration of $A\beta_{1-42}$ used in the current study exceeds physiologic concentrations, which are thought to lie in the low-nanomolar range, although accumulation of $A\beta_{1-42}$ in micro-molar ranges can occur. Therefore, the generalization of our findings to strictly physiologic conditions should be made with caution, and future work using nanomolar $A\beta_{1-42}$ could determine the extent to which the same mitochondrial calcium responses are generated. Finally, Sanz-Blasco *et al.* find a similar increase in mitochondrial calcium, using mitochondria-targeted aequorin as a calcium probe.[79] Our findings align with existing literature, highlighting the sensitivity and specificity of mt-Fura-2.3 AM for mitochondrial calcium measurement.

Further studies support the idea that inhibiting ferroptosis can protect against mitochondrial damage. Ye *et al.* demonstrated that liproxstatin-1 protects mitochondria from damage induced by glycoxylate in HK-2 cells.[80] In our study, Fer-1 pretreatment in PCNs inhibited the mitochondrial calcium increase and subsequent calcium oscillations caused by $A\beta_{1-42}$, indicating that ferroptosis plays a role in mitochondrial dysfunction. $A\beta_{1-42}$ stimulates glutamate release and inhibits its recycling, leading to increased glutamate levels.[81,82] This may impair the GSH-pathway and reduce GPx4 activity, which normally helps to inhibit ferroptosis by reducing oxidized PUFAs.[83] Fer-1 inhibits formation of these oxidized PUFAs, thereby preventing ROS formation and ferroptosis. This mechanism could explain how ferroptosis inhibition by Fer-1 might mitigate Aβ toxicity. Supporting this, Chen *et al.* found that overexpressing GPx4 in 5xFAD mice reduces $A\beta_{1-42}$ levels, further highlighting the role of ferroptosis in $A\beta_{1-42}$ toxicity.[32]

Pretreatment of the PCNs with MCU-inhibitor MCU-i4 rescued both the initial increase and the calcium oscillations following addition of $A\beta_{1-42}$. This confirms that the measured mitochondrial calcium is related to mitochondrial calcium, not cytosolic calcium as MCU-i4 inhibits calcium influx to the mitochondrial matrix. It also suggests that although calcium influx to the cytosol is increased due to $A\beta_{1-42}$ pore formation at the plasma membranes, the main calcium influx to the mitochondria occurs through the MCU, not similar pores. This is in line with the findings of Calvo-Rodriguez *et al.*, showing that blockage of the MCU using ruthenium 360 (Ru360) inhibits the increase in mitochondrial calcium resulting from $A\beta_{1-42}$ addition.[84]

The neuronal activity was increased by $A\beta_{1-42}$, which could be prevented by MCU-i4 but not Fer-1 pre-treatment. The rise in neuronal firing following $A\beta_{1-42}$ treatment might be due to an increase in active synapses and neurotransmitter release. This could be a result of modulating calcium channels and enhancing calcium uptake, which may promote synaptic vesicle release and neuronal excitability.[85,86] This aligns with our findings of increased mitochondrial calcium following $A\beta_{1-42}$ treatment. However, Aβ could also induce membrane

disruption by creating pores and altering ion homeostasis, making cells more likely to depolarize.[87,88] Additionally, Aβ can induce an imbalance of sodium and potassium channels, increasing their activity, leading to increased neuronal excitability.[89] This effect was observed in primary mouse astrocytes, suggesting it could also occur in other brain cells like neurons and oligodendrocytes.[90] However, this imbalance was induced by $A\beta_{25-35}$ and $A\beta_{1-40}$ but not by $A\beta_{1-42}$, the latter being the form used in our study. $A\beta_{1-42}$ could also act on NMDA and AMPA receptors, further enhancing glutamate release and inhibiting glutamate reuptake, which could also cause increased neuronal firing.[91] To eliminate this having an influence on the results after $A\beta_{1-42}$ treatment, HT22 cells could be used since they lack these receptors. However, HT22 cells do not develop a mature neuronal network, which would prevent the analysis of axonal mitochondrial transport as performed in our model. Fer-1 did not protect against the $A\beta_{1-42}$-induced neuronal firing, which aligns with its mode of action, as Fer-1 acts intracellularly rather than at the cell membrane level. Additionally, our results showing that MCU inhibition can reduce $A\beta_{1-42}$-induced neuronal firing are consistent with recent studies reporting that MCU potentiates the excitability of pyramidal neurons,[92] and that MCU deficiency can protect against hyperexcitability by modulating the ROS balance,[93] further supporting our data.

Using a two-compartment microfluidic device which represents a sophisticated model for isolating the neuronal network from the somal compartment, enables precise tracking of mitochondrial movement in cortical neurons. This model offers significant advantages, including the ability to determine whether mitochondria are traveling from the soma to the axonal terminal or *vice versa*. Another key advantage is the capacity to selectively treat distinct neuronal compartments. In our study, treating only the somal compartment with a high concentration of a ferroptosis inducer resulted in axonal degeneration and disruption of the neuronal network. Similarly, treating the neuronal network compartment either with a ferroptosis inducer or $A\beta_{1-42}$ to mimic $A\beta_{1-42}$ toxicity in the cortex, led to noticeable changes in mitochondrial movement. This selective treatment approach differs from traditional methods where all somas and neuronal networks in a dish are treated simultaneously, thus offering greater control over the experimental conditions and directionality of cellular responses. Another major strength of this study is the use of the novel mitochondria-specific calcium probe, mt-Fura-2.3AM for imaging mitochondrial calcium in PCN. The use of a ratiometric probe benefits the study, as this ratio compensates for the shape of the mitochondria and can be used to make an accurate comparison between several treatments. Additionally, this study allows precise measurements of mitochondrial calcium and supports its involvement in ferroptosis in the context of AD-related $A\beta_{1-42}$ toxicity. Another strength is the method of using live cell imaging, which will lay a good foundation for studies with organ-on-a-chip methods, in particular brain-on-a-chip.

The fact that mitochondria, under increased vulnerability to ferroptosis and $A\beta_{1-42}$ toxicity, return to the soma could be explained by potential increased mitophagy in AD.[27–29] Alternatively, it is possible that mitochondria do not return to the soma solely for mitophagy. Instead, they may be involved in housekeeping mechanisms that help retract the axon, save energy, and maintain vital metabolic processes, allowing the cell to survive without undergoing cell death.[94]

In conclusion, our findings highlight the critical role of ferroptosis in AD, demonstrating its impact on mitochondrial movement, calcium regulation, and neuronal activity. We suggest that ferroptosis inhibition may provide a therapeutic strategy to mitigate Aβ-mediated dysfunctions in AD pathology.

Author contributions

NM, AMD, and WD designed the theme of the manuscript. NM, MK contributed by acquiring raw data, performing the analysis and writing of this manuscript. BC and DM characterized the heterogeneous movement of mitochondria at basal conditions under the supervision of CÅ. YZ contributed to the MEA experiments. TC provided support with culturing PCNs. PPMFAM and EV provided support for development of the microfluidic chip. AM designed and performed the synthesis of mt-Fura-2.3AM probe. AM, DP and CM provided tools to measure mitochondrial calcium. AMD, WD and CÅ conducted critical revisions of the manuscript. All authors contributed to the article and approved the submitted version.

Conflicts of interest

The authors declare that the research was conducted in the absence of any commercial or financial relationships that could be construed as a potential conflict of interest.

Data availability

The data supporting the conclusions drawn in this manuscript are contained within the article and supplementary information (SI). Further inquiries may be directed to the corresponding author.

Supplementary information is available. See DOI: https://doi.org/10.1039/d5lc00834d.

Acknowledgements

NM received a De Cock research grant and a fellowship from the Behavioural and Cognitive Neuroscience Graduate School, University Medical Centre Groningen. BC was supported by a scholarship awarded under the Advanced Materials theme of the Faculty of Science and Engineering, University of Groningen. AMD is the recipient of an Alzheimer Nederland grant (WE.03- 2018-04, Netherlands), and a Rosalind Franklin

Fellowship co-funded by the European Union and the University of Groningen. We would like to thank the UMCG Microscopy and Imaging Center (UMIC) for their assistance in establishing the imaging of mitochondrial movement.

References

1 P. Lei, S. Ayton and A. I. Bush, The essential elements of Alzheimer's disease, *J. Biol. Chem.*, 2021, **296**, 100105.
2 C. Y. Ewald and C. Li, The secreted Alzheimer-related amyloid precursor protein fragment has an essential role in C. elegans, *Prion*, 2012, **6**(5), 433–436.
3 M. Medina, F. Hernández and J. Avila, New features about tau function and dysfunction, *Biomolecules*, 2016, **6**(2), 1–12.
4 G. Landreth, C. Combs, J. C. Karlo and S. Sundararajan, Inflammatory Mechanisms in Alzheimer's Disease: β-Amyloid-Stimulated Proinflammatory Responses are Blocked by PPARγ Agonists, *J. Neurosci.*, 2002, **20**(2), 163–168.
5 S. Hauptmann, I. Scherping, S. Dröse, U. Brandt, K. L. Schulz and M. Jendrach, *et al.*, Mitochondrial dysfunction: An early event in Alzheimer pathology accumulates with age in AD transgenic mice, *Neurobiol. Aging*, 2009, **30**(10), 1574–1586.
6 H. Verma, P. Gangwar, A. Yadav, B. Yadav, R. Rao and S. Kaur, *et al.*, Understanding the neuronal synapse and challenges associated with the mitochondrial dysfunction in mild cognitive impairment and Alzheimer's disease, *Mitochondrion*, 2023, **73**, 19–29.
7 T. Song, X. Song, C. Zhu, R. Patrick, M. Skurla and I. Santangelo, *et al.*, Mitochondrial dysfunction, oxidative stress, neuroinflammation, and metabolic alterations in the progression of Alzheimer's disease: A meta-analysis of in vivo magnetic resonance spectroscopy studies, *Ageing Res. Rev.*, 2021, **72**, 1–33.
8 K. Hirai, G. Aliev, A. Nunomura, H. Fujioka, R. L. Russell and C. S. Atwood, *et al.*, Mitochondrial abnormalities in Alzheimer's disease, *J. Neurosci.*, 2001, **21**(9), 3017–3023.
9 M. J. Calkins and P. H. Reddy, Amyloid beta impairs mitochondrial anterograde transport and degenerates synapses in Alzheimer's disease neurons, *Biochim. Biophys. Acta, Mol. Basis Dis.*, 2011, **1812**(4), 507–513.
10 M. Trombetta-Lima, A. M. Sabogal-Guáqueta and A. M. Dolga, Mitochondrial dysfunction in neurodegenerative diseases: A focus on iPSC-derived neuronal models, *Cell Calcium*, 2021, **94**, 102362.
11 I. E. Krabbendam, B. Honrath, B. Dilberger, E. F. Iannetti, R. S. Branicky and T. Meyer, *et al.*, SK channel-mediated metabolic escape to glycolysis inhibits ferroptosis and supports stress resistance in C. elegans, *Cell Death Dis.*, 2020, **11**(4), 263.
12 M. A. Greenough, D. J. R. Lane, R. Balez, H. T. D. Anastacio, Z. Zeng and K. Ganio, *et al.*, Selective ferroptosis vulnerability due to familial Alzheimer's disease presenilin mutations, *Cell Death Differ.*, 2022, **29**(11), 2123–2136.
13 D. J. R. Lane, S. Ayton and A. I. Bush, Iron and Alzheimer's Disease: An Update on Emerging Mechanisms, *J. Alzheimer's Dis.*, 2018, **64**(s1), S379–S395.
14 N. Majerníková, W. F. A. den Dunnen and A. M. Dolga, The Potential of Ferroptosis-Targeting Therapies for Alzheimer's Disease: From Mechanism to Transcriptomic Analysis, *Front. Aging Neurosci.*, 2021, **13**, 1–14.
15 P. Maher, K. van Leyen, P. N. Dey, B. Honrath, A. Dolga and A. Methner, The role of Ca2+ in cell death caused by oxidative glutamate toxicity and ferroptosis, *Cell Calcium*, 2018, **70**, 47–55.
16 S. Neitemeier, A. Jelinek, V. Laino, L. Hoffmann, I. Eisenbach and R. Eying, *et al.*, BID links ferroptosis to mitochondrial cell death pathways, *Redox Biol.*, 2017, **12**, 558–570.
17 J. Becerril-Ortega, K. Bordji, T. Fréret, T. Rush and A. Buisson, Iron overload accelerates neuronal amyloid-β production and cognitive impairment in transgenic mice model of Alzheimer's disease, *Neurobiol. Aging*, 2014, **35**(10), 2288–2301.
18 C. D. Sanmartín, P. Veloso, T. Adasme, P. Lobos, B. Bruna and J. Galaz, *et al.*, RyR2-mediated Ca2+ release and mitochondrial ROS generation partake in the synaptic dysfunction caused by amyloid β peptide oligomers, *Front. Mol. Neurosci.*, 2017, **10**, 1–17.
19 J. Ryu, K. Girigoswami, C. Ha, S. H. Ku and C. B. Park, Influence of multiple metal ions on β-amyloid aggregation and dissociation on a solid surface, *Biochemistry*, 2008, **47**(19), 5328–5335.
20 M. Renner, P. N. Lacor, P. T. Velasco, J. Xu, A. Contractor and W. L. Klein, *et al.*, Deleterious Effects of Amyloid β Oligomers Acting as an Extracellular Scaffold for mGluR5, *Neuron*, 2010, **66**(5), 739–754.
21 M. Arbel-Ornath, E. Hudry, J. R. Boivin, T. Hashimoto, S. Takeda and K. V. Kuchibhotla, *et al.*, Soluble oligomeric amyloid-β induces calcium dyshomeostasis that precedes synapse loss in the living mouse brain, *Mol. Neurodegener.*, 2017, **12**(1), 1–14.
22 O. Simakova and N. J. Arispe, Early and late cytotoxic effects of external application of the Alzheimer's Aβ result from the initial formation and function of Aβ ion channels, *Biochemistry*, 2006, **45**(18), 5907–5915.
23 H. Zhang, C. Knight, S. R. W. Chen and I. Bezprozvanny, A Gating Mutation in Ryanodine Receptor Type 2 Rescues Phenotypes of Alzheimer's Disease Mouse Models by Upregulating Neuronal Autophagy, *J. Neurosci.*, 2023, **43**(8), 1441–1454.
24 S. Gleitze, O. A. Ramírez, I. Vega-Vásquez, J. Yan, P. Lobos and H. Bading, *et al.*, Ryanodine Receptor Mediated Calcium Release Contributes to Ferroptosis Induced in Primary Hippocampal Neurons by GPX4 Inhibition, *Antioxidants*, 2023, **12**(3), 705.
25 A. Marmolejo-Garza, I. E. Krabbendam, M. D. A. Luu, F. Brouwer, M. Trombetta-Lima and O. Unal, *et al.*, Negative modulation of mitochondrial calcium uniporter complex protects neurons against ferroptosis, *Cell Death Dis.*, 2023, **14**(11), 772.
26 C. Hung, Importance of retrograde axonal transport in mitochondrial health and distribution, *Cell Death Discovery*, 2021, **7**(1), 7–8.

27 A. Mandal, H. T. C. Wong, K. Pinter, N. Mosqueda, A. Beirl and R. M. Lomash, *et al.*, Retrograde mitochondrial transport is essential for organelle distribution and health in Zebrafish Neurons, *J. Neurosci.*, 2021, **41**(7), 1371–1392.

28 P. Martín-Maestro, R. Gargini, G. Perry, J. Avila and V. García-Escudero, PARK2 enhancement is able to compensate mitophagy alterations found in sporadic Alzheimer's disease, *Hum. Mol. Genet.*, 2016, **25**(4), 792–806.

29 J. S. Kerr, B. A. Adriaanse, N. H. Greig, M. P. Mattson, M. Z. Cader and V. A. Bohr, *et al.*, Mitophagy and Alzheimer's Disease: Cellular and Molecular Mechanisms, *Trends Neurosci.*, 2017, **40**(3), 151–166.

30 M. de la Cueva, D. Antequera, L. Ordoñez-Gutierrez, F. Wandosell, A. Camins and E. Carro, *et al.*, Amyloid-β impairs mitochondrial dynamics and autophagy in Alzheimer's disease experimental models, *Sci. Rep.*, 2022, **12**(1), 1–15.

31 S. Li, S. Hong, N. E. Shepardson, D. M. Walsh, G. M. Shankar and D. Selkoe, Soluble Oligomers of Amyloid β Protein Facilitate Hippocampal Long-Term Depression by Disrupting Neuronal Glutamate Uptake, *Neuron*, 2009, **62**(6), 788–801.

32 L. Chen, N. J. Dar, R. Na, K. D. McLane, K. Yoo and X. Han, *et al.*, Enhanced defense against ferroptosis ameliorates cognitive impairment and reduces neurodegeneration in 5xFAD mice, *Free Radical Biol. Med.*, 2022, **180**, 1–12.

33 A. Seiler, M. Schneider, H. Förster, S. Roth, E. K. Wirth and C. Culmsee, *et al.*, Glutathione Peroxidase 4 Senses and Translates Oxidative Stress into 12/15-Lipoxygenase Dependent- and AIF-Mediated Cell Death, *Cell Metab.*, 2008, **8**(3), 237–248.

34 P. K. Mandal, S. Saharan, M. Tripathi and G. Murari, Brain Glutathione Levels - A Novel Biomarker for Mild Cognitive Impairment and Alzheimer's Disease, *Biol. Psychiatry*, 2015, **78**(10), 702–710.

35 E. M. Öxler, A. Dolga and C. Culmsee, AIF depletion provides neuroprotection through a preconditioning effect, *Apoptosis*, 2012, **17**(10), 1027–1038.

36 Y. Zhang, S. Shaabani, K. Vowinkel, M. Trombetta-Lima, A. M. Sabogal-Guáqueta and T. Chen, *et al.*, Novel SK channel positive modulators prevent ferroptosis and excitotoxicity in neuronal cells, *Biomed. Pharmacother.*, 2024, **171**, 116163.

37 A. M. Dolga, N. Terpolilli, F. Kepura, I. M. Nijholt, H. G. Knaus and B. D'Orsi, *et al.*, KCa2 channels activation prevents [Ca2+]i deregulation and reduces neuronal death following glutamate toxicity and cerebral ischemia, *Cell Death Dis.*, 2011, **2**(4), 1–10.

38 J. Schindelin, I. Arganda-Carreras, E. Frise, V. Kaynig, M. Longair and T. Pietzsch, *et al.*, Fiji: An open-source platform for biological-image analysis, *Nat. Methods*, 2012, **9**(7), 676–682.

39 C. A. Schneider, W. S. Rasband and K. W. Eliceiri, NIH Image to ImageJ: 25 years of image analysis, *Nat. Methods*, 2012, **9**(7), 671–675.

40 J. Y. Tinevez, N. Perry, J. Schindelin, G. M. Hoopes, G. D. Reynolds and E. Laplantine, *et al.*, TrackMate: An open and extensible platform for single-particle tracking, *Methods*, 2017, **115**(2017), 80–90.

41 B. Corci, O. Hooiveld, A. M. Dolga and C. Åberg, Extending the analogy between intracellular motion in mammalian cells and glassy dynamics, *Soft Matter*, 2023, **19**(14), 2529–2538.

42 C. Åberg and B. Poolman, Glass-like characteristics of intracellular motion in human cells, *Biophys. J.*, 2021, **120**(11), 2355–2366.

43 T. Chen, N. Majerníková, A. Marmolejo-Garza, M. Trombetta-Lima, A. M. Sabogal-Guáqueta and Y. Zhang, *et al.*, Mitochondrial transplantation rescues neuronal cells from ferroptosis, *Free Radical Biol. Med.*, 2023, **208**, 62–72.

44 P. A. Goldsteen, A. M. Sabogal Guaqueta, P. P. M. F. A. Mulder, I. S. T. Bos, M. Eggens and L. Van der Koog, *et al.*, Differentiation and on axon-guidance chip culture of human pluripotent stem cell-derived peripheral cholinergic neurons for airway neurobiology studies, *Front. Pharmacol.*, 2022, **13**, 1–16.

45 D. Pendin, R. Norante, A. De Nadai, G. Gherardi, N. Vajente and E. Basso, *et al.*, A Synthetic Fluorescent Mitochondria-Targeted Sensor for Ratiometric Imaging of Calcium in Live Cells, *Angew. Chem., Int. Ed.*, 2019, **58**(29), 9917–9922.

46 A. Alsina, W. M. Lai, W. K. Wong, X. Qin, M. Zhang and H. Park, Real-time subpixel-accuracy tracking of single mitochondria in neurons reveals heterogeneous mitochondrial motion, *Biochem. Biophys. Res. Commun.*, 2017, **493**(1), 776–782.

47 Y. Zhang, B. Y. Fan, Y. L. Pang, W. Y. Shen, X. Wang and C. X. Zhao, *et al.*, Neuroprotective effect of deferoxamine on erastininduced ferroptosis in primary cortical neurons, *Neural Regener. Res.*, 2020, **15**(8), 1539–1545.

48 E. Perlson, G. B. Jeong, J. L. Ross, R. Dixit, K. E. Wallace and R. G. Kalb, *et al.*, A switch in retrograde signaling from survival to stress in rapid-onset neurodegeneration, *J. Neurosci.*, 2009, **29**(31), 9903–9917.

49 S. H. Berth and T. E. Lloyd, Disruption of axonal transport in neurodegeneration, *J. Clin. Invest.*, 2023, **133**(11), 1–12.

50 K. Palikaras, E. Lionaki and N. Tavernarakis, Coordination of mitophagy and mitochondrial biogenesis during ageing in C. elegans, *Nature*, 2015, **521**(7553), 525–528.

51 Y. Xia, X. Sun, Y. Luo and C. M. Stary, Ferroptosis contributes to isoflurane neurotoxicity, *Front. Mol. Neurosci.*, 2019, **11**, 1–7.

52 P. R. Angelova, M. L. Choi, A. V. Berezhnov, M. H. Horrocks, C. D. Hughes and S. De, *et al.*, Alpha synuclein aggregation drives ferroptosis: an interplay of iron, calcium and lipid peroxidation, *Cell Death Differ.*, 2020, **27**(10), 2781–2796.

53 R. Frazão, D. G. McMahon, W. Schunack, P. Datta, R. Heidelberger and D. W. Marshak, Histamine elevates free intracellular calcium in mouse retinal dopaminergic cells via H1-receptors, *Invest. Ophthalmol. Visual Sci.*, 2011, **52**(6), 3083–3088.

54 N. Esteras and A. Y. Abramov, Mitochondrial calcium deregulation in the mechanism of beta-amyloid and Tau pathology, *Cell*, 2020, **9**(9), 1–17.

55 O. Stoler, A. Stavsky, Y. Khrapunsky, I. Melamed, G. Stutzmann and D. Gitler, *et al.*, Frequency-and spike-timing-dependent mitochondrial Ca2+ signaling regulates the metabolic rate and synaptic efficacy in cortical neurons, *eLife*, 2022, **11**, 1–14.

56 D. Yamazaki, M. Aoyama, S. Ohya, K. Muraki, K. Asai and Y. Imaizumi, Novel functions of small conductance Ca2+ −activated K + channel in enhanced cell proliferation by ATP in brain endothelial cells, *J. Biol. Chem.*, 2006, **281**(50), 38430–38439.

57 J. T. Neary, R. Laskey, C. van Breemen, J. Blicharska, L. O. B. Norenberg and M. D. Norenberg, ATP-evoked calcium signal stimulates protein phosphorylation/dephosphorylation in astrocytes, *Brain Res.*, 1991, **566**(1–2), 89–94.

58 M. W. Salter and J. L. Hicks, ATP-evoked increases in intracellular calcium in neurons and glia from the dorsal spinal cord, *J. Neurosci.*, 1994, **14**(3 II), 1563–1575.

59 M. Richter, N. Vidovic, K. Biber, A. Dolga, C. Culmsee and R. Dodel, The neuroprotective role of microglial cells against amyloid beta-mediated toxicity in organotypic hippocampal slice cultures, *Brain Pathol.*, 2020, **30**(3), 589–602.

60 Y. Zhang, B. Y. Fan, Y. L. Pang, W. Y. Shen, X. Wang, C. X. Zhao, W. X. Li, C. Liu, X. H. Kong, G. Z. Ning, S. Q. Feng and X. Yao, Neuroprotective effect of deferoxamine on erastin induced ferroptosis in primary cortical neurons, *Neural Regener. Res.*, 2020, **15**(8), 1539–1545.

61 G. Miotto, M. Rossetto, M. L. Di Paolo, L. Orian, R. Venerando, A. Roveri, A. M. Vučković, V. Bosello Travain, M. Zaccarin, L. Zennaro, M. Maiorino, S. Toppo, F. Ursini and G. Cozza, Insight into the mechanism of ferroptosis inhibition by ferrostatin-1, *Redox Biol.*, 2020, **28**, 101328.

62 M. Zille, A. Kumar, N. Kundu, M. W. Bourassa, V. S. C. Wong, D. Willis, S. S. Karuppagounder and R. R. Ratan, Ferroptosis in Neurons and Cancer Cells Is Similar But Differentially Regulated by Histone Deacetylase Inhibitors, *eNeuro*, 2019, **6**(1), ENEURO.0263-18.

63 L. A. Ligon and O. Steward, Role of microtubules and actin filaments in the movement of mitochondria in the axons and dendrites of cultured hippocampal neurons, *J. Comp. Neurol.*, 2000, **427**(3), 351–361.

64 X. Wang, G. Guo, J. Zhang, N. Aebez, Z. Liu and C. F. Liu, *et al.*, Mutant-TMEM230-induced neurodegeneration and impaired axonal mitochondrial transport, *Hum. Mol. Genet.*, 2021, **30**(16), 1535–1542.

65 R. F. Simões, R. Pino, M. Moreira-Soares, J. Kovarova, J. Neuzil and R. Travasso, *et al.*, Quantitative analysis of neuronal mitochondrial movement reveals patterns resulting from neurotoxicity of rotenone and 6-hydroxydopamine, *FASEB J.*, 2021, **35**(12), 1–16.

66 F. Wehnekamp, G. Plucińska, R. Thong, T. Misgeld and D. C. Lamb, Nanoresolution real-time 3D orbital tracking for studying mitochondrial trafficking in vertebrate axons in vivo, *eLife*, 2019, **8**, 1–22.

67 A. Mandal, K. Pinter, N. Mosqueda, A. Beirl, R. M. Lomash and S. Won, *et al.*, Retrograde mitochondrial transport is essential for mitochondrial homeostasis in neurons, *J. Neurosci.*, 2021, **41**(7), 1371–1392.

68 S. H. Berth and T. E. Lloyd, Disruption of axonal transport in neurodegeneration, *J. Clin. Invest.*, 2023, **133**(11), e168554.

69 E. C. Kimball, M. E. Pease, M. R. Steinhart, E. N. Oglesby, I. Pitha and C. Nguyen, *et al.*, A mouse ocular explant model that enables the study of living optic nerve head events after acute and chronic intraocular pressure elevation: Focusing on retinal ganglion cell axons and mitochondria, *Exp. Eye Res.*, 2017, **160**, 106–115.

70 A. Sabui, M. Biswas, P. R. Somvanshi, P. Kandagiri, M. Gorla and F. Mohammed, *et al.*, Decreased anterograde transport coupled with sustained retrograde transport contributes to reduced axonal mitochondrial density in tauopathy neurons, *Front. Mol. Neurosci.*, 2022, **15**, 1–14.

71 V. H. Sánchez-Vázquez, E. Martínez-Martínez, M. L. Gallegos-Gómez, J. M. Arias, G. Pallafacchina and R. Rizzuto, *et al.*, Heterogeneity of the endoplasmic reticulum Ca2+ store determines colocalization with mitochondria, *Cell Calcium*, 2023, **109**, 102688.

72 S. S. V. P. Sakamuri, V. N. Sure, X. Wang, G. Bix, V. A. Fonseca and R. Mostany, *et al.*, Amyloid β (1–42) peptide impairs mitochondrial respiration in primary human brain microvascular endothelial cells: impact of dysglycemia and pre-senescence, *GeroScience*, 2022, **44**(6), 2721–2739.

73 D. D. Quintana, J. A. Garcia, Y. Anantula, S. L. Rellick, E. B. Engler-Chiurazzi and S. N. Sarkar, *et al.*, Amyloid-β Causes Mitochondrial Dysfunction via a Ca2+-Driven Upregulation of Oxidative Phosphorylation and Superoxide Production in Cerebrovascular Endothelial Cells, *J. Alzheimer's Dis.*, 2020, **75**(1), 119–138.

74 L. Naia, M. Shimozawa, E. Bereczki, X. Li, J. Liu and R. Jiang, *et al.*, Mitochondrial hypermetabolism precedes impaired autophagy and synaptic disorganization in App knock-in Alzheimer mouse models, *Mol. Psychiatry*, 2023, **28**(9), 3966–3981.

75 M. Kato-Negishi and M. Kawahara, Neurosteroids block the increase in intracellular calcium level induced by Alzheimer's β-amyloid protein in long-term cultured rat hippocampal neurons, *Neuropsychiatr. Dis. Treat.*, 2008, **4**(1 B), 209–218.

76 E. F. Shevtsova, P. R. Angelova, O. A. Stelmashchuk, N. Esteras, N. A. Vasil'eva and A. V. Maltsev, *et al.*, Pharmacological sequestration of mitochondrial calcium uptake protects against dementia and β-amyloid neurotoxicity, *Sci. Rep.*, 2022, **12**(1), 1–17.

77 M. Calvo-Rodriguez, M. Garcia-Durillo, C. Villalobos and L. Nunez, Aging enables Ca2+ overload and apoptosis induced by amyloid-β oligomers in rat hippocampal neurons: Neuroprotection by non-steroidal anti-inflammatory drugs and r-flurbiprofen in aging neurons, *J. Alzheimer's Dis.*, 2016, **54**(1), 207–221.

78 R. I. Fonteriz, S. de la Fuente, A. Moreno, C. D. Lobatón, M. Montero and J. Alvarez, Monitoring mitochondrial [Ca2+] dynamics with rhod-2, ratiometric pericam and aequorin, *Cell Calcium*, 2010, **48**(1), 61–69.

79 S. Sanz-Blasco, R. A. Valero, I. Rodríguez-Crespo, C. Villalobos and L. Núñez, Mitochondrial Ca2+ overload underlies Aβ oligomers neurotoxicity providing an unexpected mechanism of neuroprotection by NSAIDs, *PLoS One*, 2008, **3**(7), e2718.

80 Z. Ye, Y. Xia, L. Li, B. Li, L. Chen and W. Yu, *et al.*, P53 Deacetylation Alleviates Calcium Oxalate Deposition-Induced Renal Fibrosis By Inhibiting Ferroptosis, *Biomed. Pharmacother.*, 2023, **164**, 114925.

81 V. Campos-Peña and M. A. Meraz-Ríos, Alzheimer Disease: The Role of Aβ in the Glutamatergic System, *Neurochemistry*, InTech, 2014, DOI: 10.5772/57367.

82 M. Talantova, S. Sanz-Blasco, X. Zhang, P. Xia, M. W. Akhtar and S. I. Okamoto, *et al.*, Aβ induces astrocytic glutamate release, extrasynaptic NMDA receptor activation, and synaptic loss, *Proc. Natl. Acad. Sci. U. S. A.*, 2013, **110**(27), E2518-27.

83 W. S. Yang, R. Sriramaratnam, M. E. Welsch, K. Shimada, R. Skouta and V. S. Viswanathan, *et al.*, Regulation of ferroptotic cancer cell death by GPX4, *Cell*, 2014, **156**(1–2), 317–331.

84 M. Calvo-Rodriguez, S. S. Hou, A. C. Snyder, E. K. Kharitonova, A. N. Russ and S. Das, *et al.*, Increased mitochondrial calcium levels associated with neuronal death in a mouse model of Alzheimer's disease, *Nat. Commun.*, 2020, **11**(1), 1–17.

85 J. R. K. Marland, P. Hasel, K. Bonnycastle and M. A. Cousin, Mitochondrial calcium uptake modulates synaptic vesicle endocytosis in central nerve terminals, *J. Biol. Chem.*, 2016, **291**(5), 2080–2086.

86 W. Cai, L. Li, S. Sang, X. Pan and C. Zhong, Physiological Roles of β-amyloid in Regulating Synaptic Function: Implications for AD Pathophysiology, *Neurosci. Bull.*, 2023, **39**(8), 1289–1308.

87 D. C. Bode, M. D. Baker and J. H. Viles, Ion channel formation by amyloid-β42 oligomers but not amyloid-β40 in cellular membranes, *J. Biol. Chem.*, 2017, **292**(4), 144–1413.

88 M. F. M. Sciacca, S. A. Kotler, J. R. Brender, J. Chen, D. K. Lee and A. Ramamoorthy, Two-step mechanism of membrane disruption by Aβ through membrane fragmentation and pore formation, *Biophys. J.*, 2012, **103**(4), 702–710.

89 V. M. Vitvitsky, S. K. Garg, R. F. Keep, R. L. Albin and R. Banerjee, Na + and K + ion imbalances in Alzheimer's disease, *Biochim. Biophys. Acta, Mol. Basis Dis.*, 2012, **1822**(11), 1671–1681.

90 W. B. Chen, Y. X. Wang, H. G. Wang, D. An, D. Sun and P. Li, *et al.*, TPEN attenuates amyloid-β_{25-35}-induced neuronal damage with changes in the electrophysiological properties of voltage-gated sodium and potassium channels, *Mol. Brain*, 2021, **14**(1), 124.

91 J. Liu, L. Chang, Y. Song, H. Li and Y. Wu, The role of NMDA receptors in Alzheimer's disease, *Front. Neurosci.*, 2019, **13**, 1–22.

92 C. J. Groten and B. A. MacVicar, Mitochondrial Ca2+ uptake by the MCU facilitates pyramidal neuron excitability and metabolism during action potential firing, *Commun. Biol.*, 2022, **5**(1), 1–15.

93 L. Bierhansl, L. Gola, V. Narayanan, A. Dik, S. G. Meuth and H. Wiendl, *et al.*, Neuronal Mitochondrial Calcium Uniporter (MCU) Deficiency Is Neuroprotective in Hyperexcitability by Modulation of Metabolic Pathways and ROS Balance, *Mol. Neurobiol.*, 2024, **61**(11), 9529–9538.

94 K. A. Chamberlain and Z. H. Sheng, Mechanisms for the maintenance and regulation of axonal energy supply, *J. Neurosci. Res.*, 2019, **97**(8), 897–913.

95 G. Di Marco, F. Vallese, B. Jourde, C. Bergsdorf, M. Sturlese, A. De Mario, V. Techer-Etienne, D. Haasen, B. Oberhauser, S. Schleeger, G. Minetti, S. Moro, R. Rizzuto, D. De Stefani, M. Fornaro and C. Mammucari, A high-throughput screening identifies MICU1 targeting compounds, *Cell Rep.*, 2020, **30**(7), 2321–2331.e6.